

ORIGINAL ARTICLE

Stem cell-derived neurons from autistic individuals with SHANK3 mutation show morphogenetic abnormalities during early development

A Kathuria¹, P Nowosiad¹, R Jagasia², S Aigner³, RD Taylor^{4,5}, LC Andreae^{4,5}, NJF Gatford¹, W Lucchesi⁶, DP Srivastava^{1,5} and J Price^{1,5,7}

Shank3 is a structural protein found predominantly at the postsynaptic density. Mutations in the *SHANK3* gene have been associated with risk for autism spectrum disorder (ASD). We generated induced pluripotent stem cells (iPSCs) from control individuals and from human donors with ASD carrying microdeletions of *SHANK3*. In addition, we used Zinc finger nucleases to generate isogenic *SHANK3* knockout human embryonic stem (ES) cell lines. We differentiated pluripotent cells into either cortical or olfactory placodal neurons. We show that patient-derived placodal neurons make fewer synapses than control cells. Moreover, patient-derived cells display a developmental phenotype: young postmitotic neurons have smaller cell bodies, more extensively branched neurites, and reduced motility compared with controls. These phenotypes were mimicked by *SHANK3*-edited ES cells and rescued by transduction with a Shank3 expression construct. This developmental phenotype is not observed in the same iPSC lines differentiated into cortical neurons. Therefore, we suggest that *SHANK3* has a critical role in neuronal morphogenesis in placodal neurons and that early defects are associated with ASD-associated mutations.

Molecular Psychiatry (2018) **23**, 735–746; doi:10.1038/mp.2017.185; published online 26 September 2017

INTRODUCTION

Autism spectrum disorder (ASD) is a group of neurodevelopmental disorders defined by restrictive repetitive behavior, deficits in social interaction and impaired communication. The etiology of ASD is not well understood. There is, however, a strong genetic basis to ASDs, as indicated by the high concordance rate between twins (up to 90% between monozygotic and 20% between dizygotic twins).¹ Between 10% and 20% of ASD patients carry pathogenic copy number variant,^{2,3} and a high proportion of these involve genes encoding synaptic proteins. This has led to the suggestion that ASD is a disorder of synaptogenesis.⁴

One such gene is *SHANK3*, which encodes a scaffolding protein of the postsynaptic density (PSD). It comprises five main domains: N terminal ankyrin repeats (ANK), PDZ domain, sterile alpha motif (SAM) domain, SRC Homology (SH3) domain, and proline-rich domain (pro).^{5,6} At the PSD, it interacts with NMDAR via the PSD95/GKAP (guanylate kinase-associated protein) complex that binds to its PDZ domain. This complex also binds the GluR1 subunit of the AMPAR (α -amino-3-hydroxy-5-methyl-4-isoxazole-propionic acid receptor). In addition, the proline-rich domain of *SHANK3* binds to the mGluR5 (metabotropic glutamate receptor) via Homer1 (Homer Scaffolding Protein 1).^{6–9} This evidence suggests that *SHANK3* recruits various synaptic receptors to the PSD and is thus a pivotal player in building the glutamatergic synapse.

The *SHANK3* gene is found at the 22q13 locus in humans, and > 1000 cases of 22q.13 deletion have been reported. In all, 75% of

these have ASD and 95% display severe developmental delay.¹⁰ Conversely, 2% of autistic individuals carry a harmful deletion in the *SHANK3* gene.^{11–13} In another cohort study carried out on 133 patients from USA and 83 patients from Italy, 5 detrimental mutations were discovered in the *SHANK3* gene with an occurrence rate of 2.3%.¹⁴ Additionally, two recent studies have shown that *SHANK3* is the most underdiagnosed, highly penetrant, monogenic cause of ASD. The first study used whole-genome sequencing to reveal a *de novo* *SHANK3* mutation in familial ASD.¹⁵ The second evaluated 32 patients and revealed *SHANK3* haploinsufficiency as the monogenic cause of ASD in 0.5% of these cases.¹⁶ Deletion in the *SHANK3* gene has been shown to cause Phelan McDermid Syndrome (PMDS), a neurodevelopmental disorder characterized by global developmental delay, speech delay, intellectual disability, poor motor coordination and ASD.¹⁷

Induced pluripotent stem cells (iPSCs) permit the study of the etiology of neurodevelopmental disorders using cells in culture to reproduce phenotypes associated with specific disease risk alleles.¹⁸ Phenotypes associated with PMDS have been studied in iPSC lines generated from two patients. This study found that iPSC-derived PMDS neurons had a reduced expression of *SHANK3* and impaired excitatory synaptic transmission.¹⁹ Both amplitude and frequency of miniature excitatory postsynaptic currents were significantly reduced, and histochemical staining revealed a decrease in both presynaptic and postsynaptic puncta, suggesting that these neurons made fewer synapses. Analysis of genetically engineered heterozygous and homozygous *SHANK3* mutations in

¹Cells & Behavior Unit, Department of Basic and Clinical Neuroscience, Institute of Psychiatry Psychology & Neuroscience, King's College London, London, UK; ²CNS Discovery/F-Hoffmann-La Roche Ltd, Basel, Switzerland; ³Department of Cellular and Molecular Medicine School of Medicine University of California, San Diego, CA, USA; ⁴Developmental Neurobiology/New Hunt's House Guy's Campus, King's College London, London, UK; ⁵MRC Centre for Neurodevelopmental Disorders, King's College London, London, UK; ⁶School of Biological Sciences, Royal Holloway, University of London, Egham, UK and ⁷Division of Advanced Therapies, National Institute for Biological Standards and Control, Hertfordshire, UK. Correspondence: Professor J Price, Cells & Behavior Unit, Department of Basic and Clinical Neuroscience, Institute of Psychiatry Psychology & Neuroscience, King's College London, London SE5 9RT, UK.

E-mail: jack.price@kcl.ac.uk

Received 31 May 2016; revised 4 July 2017; accepted 19 July 2017; published online 26 September 2017

Figure 1. Neuralization (a). The chart depicts the neuralization protocol used and indicates the five stages of neuralization. These are the induced pluripotent stem (iPS) cell (day 0), the neural progenitors (day 12), the rosette structure (day 18/19), the doublecortin positive neurons (day 26) and the synaptically active neuronal stage (day 70). (b) Day 30 placodal control neurons positive for Lhx6, Gnrh1, MAP2, DAPI (4,6-diamidino-2-phenylindole) and negative for CTIP2 (scale = 25 μm). (c) Number of Gnrh1-positive cells/total no. of nuclei. (d) Number of Lhx6-positive cells/total no. of nuclei. (e) Number of both Lhx6- and Gnrh1-positive cells/total no. of nuclei. (f) Cortical gene expression for control cortical neurons at day 30 of neuralization. (g) Olfactory placodal gene expression for control placodal neurons at day 28 of neuralization. Both graphs show fold change relative to day 0 control P1 C2, assessed via quantitative PCR (qPCR). (h) *SHANK3* fold change for control and *SHANK3* neurons at days 15, 25 and 40 of neuralization, relative to Control P2 C3 at day 15, assessed via qPCR. Data are expressed as mean \pm s.e.m. (i) Western blotting of *SHANK3* at day 30, normalized to glyceraldehyde 3-phosphate dehydrogenase (GAPDH). Three control lines were compared with 2 *SHANK3* lines with two biological replicates, Control P1 C2 stands for Control patient 1 clone, Control P2 C2 stands for Control patient 2 clone 2, Control P5 is control patient 5 and *SHANK3* P1 C1 is *SHANK3* patient 1 clone1 and *SHANK3* P2 C1 is *SHANK3* patient 2 clone 1.

human neurons has revealed alterations in neuronal morphology and synaptic connectivity. Specifically, the I_h channel is severely impaired.²⁰ Both these studies examined cortical neurons and focused on the later stages of neuronal development, as the neurons become synaptically active.

Shank3 knockout mice have also demonstrated utility in elucidating elements of ASD.^{21–25} These mice exhibit abnormal behavior, synaptic dysfunction, abnormal spine morphology, synapse formation and deficits in learning. Both the animal and iPSC studies of *SHANK3* indicate that ASD risk alleles are associated with synaptic deficits. This tends to confirm the synaptogenic deficit hypothesis for autism. No studies, however, have examined neural development at stages before the onset of synaptogenesis, even though we know that *SHANK3* is expressed from neural tube stages *in vivo*.²⁶ The question remains, therefore, of when *SHANK3* deletions first impact neural development and what role any putative early phenotypes might have on later synaptogenesis?

Most autism studies focus on neuronal defects within cortex, hippocampus and striatum. Nevertheless, there is evidence that the hypothalamus may be important in ASD. An MRI study where 52 autistic children were compared with 52 matched controls found diminished gray matter in the hypothalamus.²⁷ Another study reported that gestational hypothyroxinemia in rodents induced impaired cortical neuronal migration. Neuronal migration deficits have been reported in autistic children.²⁸ Thyroid-stimulating hormone is produced by the hypothalamus and regulates thyroid hormone production.²⁹ Moreover, low levels of thyroid-stimulating hormone during mid-pregnancy have been shown to increase significantly the odds of a child being diagnosed with autism.³⁰ Using mass spectrometry and liquid chromatography, the concentrations of three sex steroid hormones, progesterone, testosterone and 17 α -hydroxy-progesterone, have been studied in autistic children. All of these were found elevated.³¹ Gonadotropin-releasing hormone (Gnrh) produced by the hypothalamus is a precursor to these hormones. All the above studies have clearly established a link between hypothalamus and autism that has not yet been investigated in human cells.

To address these issues, we track the development trajectory of Gnrh+ neurons (as derived from the olfactory placode) generated from human iPSCs lines. These lines were produced from hair root biopsies from two categories of individuals: three healthy control individuals and two autistic patients with heterozygous deletions in the *SHANK3* gene.³² iPSCs were differentiated into neurons and their structural and functional development was tracked during the various stages of neuralization. The study reveals that, during early neuronal development, *SHANK3* iPSC-derived neurons have a smaller cell soma but more and longer primary neurites than control cells. Further, embryonic stem (ES) cell lines engineered to carry homozygous or heterozygous deletions of the *SHANK3* gene give rise to neurons with similar morphogenetic deficits to those seen in the *SHANK3* patient neurons. Not only were the morphogenetic deficits in iPSCs rescued by overexpressing *SHANK3*, but later synaptic deficits were similarly rescued by this

overexpression. Thus this study presents the novel idea that haploinsufficiency of *SHANK3* during early neuronal development compromises the structural integrity of neurons and leads to later synaptic deficits in mature neurons.

MATERIALS AND METHODS

iPSC generation and olfactory placodal neuronal differentiation

The iPSC clones were generated using a lentiviral construct from keratinocytes from two individuals with ASD and three healthy individuals, as previously reported³² (Supplementary Table 1 and 2). Neural differentiation of iPSCs was performed using the modified version dual SMAD inhibition protocol.³³ Briefly, with cells at 100% confluency, the medium was changed to N2/B27, and SMAD and Wnt agonist were added (SB431542-10 μM , XAV939-2 μM and Dorsomorphin 1 μM). Thereafter, the medium was supplemented with SMAD inhibitors and changed every day for 7 days. On day 8, the cells were split 1:1 onto geltrex substrate, giving rise to a sheet of neural progenitor cells. The cells were then fed alternate days with N2/B27 and once confluent they were split. On day 20, the cells were transferred to polyD-lysine and laminin (10 $\mu\text{g ml}^{-1}$), DAPT 10 μM and B27 media to differentiate into neurons. Immature neurons emerged around day 26. Control neurons generated from this protocol show normal neuronal electrical activity as shown in Supplementary Figure 1.

High-content image screening

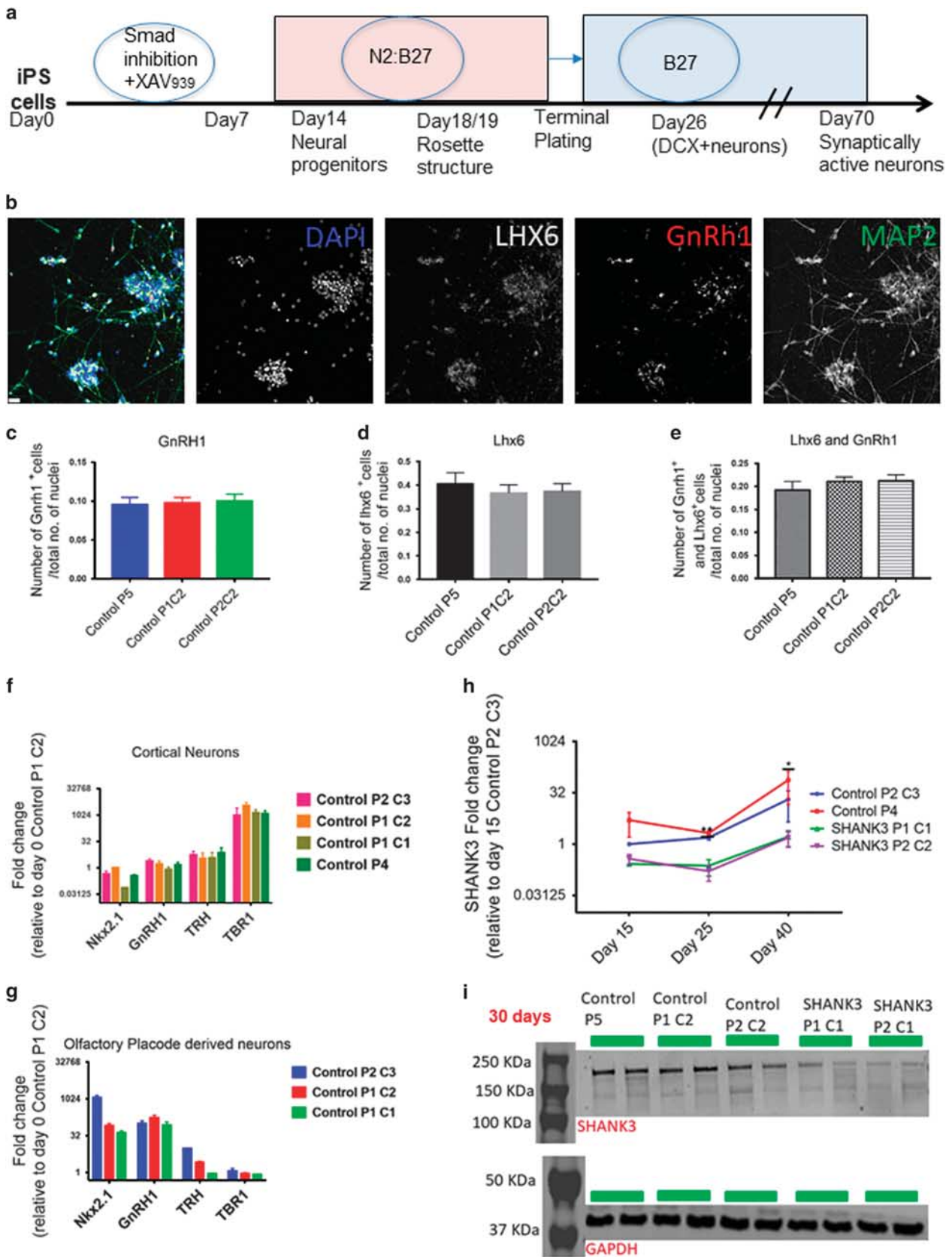
Dissociated neurons were plated at 1–1.5 $\times 10^3$ neurons per well on polyD-lysine and laminin-coated 96-well tissue culture plates. The cells were fixed and stained for neuronal markers Tuj1 (Biolegend, Berkshire, UK) and DCX (doublecortin; Abcam, Cambridge, UK). A quantitative imaging analysis of the young neurons was conducted through the Cell Insight machine at $\times 10$ magnification using the Cell Scan software (Cellomics NX11110, Pittsburgh, PA, USA). The following morphological features were assessed for both the patient and control: cell soma area and the number of primary neurites per neuron. At least 10 fields were randomly selected and scanned per well of a 96-well dish. To identify and remove any false readings generated by the Cell Insight, three random *SHANK3* and control wells were selected and counted manually (blind to genotype). A histogram was generated from the manual count depicting the distribution of the cell soma area for both control and *SHANK3* at day 30 of neuralization. The average error rate percentage is shown in Supplementary Figure 8.

Neurite outgrowth assay via time-lapse imaging

Neurons were grown on 15 mm glass bottom dish (Ibidi, Planegg, Germany) and placed in an environmentally controlled stage. Time-lapse images of cells were taken over a period of 48 h at $\times 20$ magnification using Nikon Biostation IM-Q (London, UK). Phase-contrast images were taken every hour for 48 h. Each neuron was then traced and measured for 12 h using the neurite outgrowth software (Metamorph, Molecular Devices, Sunnyvale, CA, USA). The following parameters were measured: primary neurite formation and elimination, primary neurite extension and retraction ($\mu\text{m h}^{-1}$), and cell soma speed ($\mu\text{m h}^{-1}$).

Immunocytochemistry

Cells were fixed with 4% paraformaldehyde, washed (3 \times) with phosphate-buffered saline, permeabilized with 0.1% triton-X (15 min room temperature) and blocked using 5% donkey serum (1 h room temperature). Primary antibodies were diluted in 1% donkey serum and applied (overnight at



4 °C). The primary antibodies used are described in Supplementary Table 3. Secondary antibodies were diluted (1:500) in 1% donkey serum and applied for 1 h at room temperature. The following secondary antibodies were used: Alexa 488, 594, and 647 (Invitrogen, Carlsbad, CA, USA). Neurons were visualized using either Olympus fluorescence microscope (Southampton, UK) or a laser scanning confocal microscope equipped with 405/488/594/633 nm lasers (Leica System, Wetzlar, Germany). Images within an experiment were acquired with identical acquisition setting at $\times 40$, $\times 63$ and $\times 100$.

Synaptic puncta measurement

Images were taken from the $63\times$ objective on a Leica TCS SP5 Confocal Laser Scanning Microscope coupled with the LAS AF lite software (Wetzlar, Germany). We used 386, 488 and 594 nm lasers, along with the appropriate excitation and emission filters. These settings were kept consistent while taking images from all cultures. Acquired images were converted into eight-bit tiff files and analyzed with the Image J software version 7.3 (Rockville, MD, USA). At least two portions of neurites, length not exceeding 50 μm were selected. This region was added to region of interest manager. Following this, the images were thresholded such that the synaptic puncta would turn black and the background would turn white. The thresholded images were then analyzed through 'Analyze Particles'. The size limit at this point was set up to $0.03\text{--}3\ \mu\text{m}^2$. This meant that only punctas with a size of $0.03\text{--}3\ \mu\text{m}^2$ would be measured. The summary from 'Analyze particles' gave the total number of punctas observed in the region of interest. These steps were repeated until the whole neuron was captured. The data obtained were analyzed as the number of punctas/50 μm .

Construction of SHANK3 lentiviral vector, production and infection

The full-length SHANK3 human cDNA was synthesized by GENEWIZ (Plainfield, NJ, USA) with Myc fused to the N terminal and then cloned into pCDH-EF1-MCS (CD502-1A System Biosciences, Palo Alto, CA, USA). The vector map and SHANK3 sequence has been provided in supplementary Figure 6. Lentiviruses were generated with a three-plasmid transfection system using Lipofectamine LTX (Life Technologies, Camarillo, CA, USA) in HEK293FT cells. Twelve hours after transfection, supernatants were collected. Viral particles were concentrated using Lenti-X concentrator (Clontech, Mountain View, CA, USA), aliquoted (100 μl) and stored at $-80\ ^\circ\text{C}$. Different amounts of virus (5–50 μl) were placed on $\sim 70\%$ confluent neurons for 2 days. Approximately 80% of the cells in one well of a 96-well dish stained positive for Myc on addition of 5 μl of virus. We used 5 μl of SHANK3-myc virus to transduce at day 20. The medium was replaced 24 h later. Neurons were analyzed after 10 days. Verification of SHANK3 overexpression virus was performed via immunocytochemistry (Supplementary Figure 7).

Genetic engineering of ES cell lines and validation (es shank3 -/- and es shank3+/-)

Constructs. Plasmids encoding a pair of zinc finger nucleases (ZFNs) targeting the 5' end of exon 21 of SHANK3 (CompoZr Custom ZFN) were from Sigma. The ZFN recognition site is GGCCCTCCGTCGAGGGGGA CGAGAAGCTGGCG, where upper and lower case letters denote the ZFN binding and cut sites, respectively. mRNA encoding ZFNs targeting exon 1 of the PPP1R12C (also known as AAVS1) locus was from Sigma (St Louis, MO, USA; CompoZr Targeted Integration Kit). Targeting constructs harboring a loxP-flanked phosphoglycerate kinase promoter (PGK)-driven neomycin phosphotransferase cassette (loxP-PGK-neo-loxP, surrounded on either side by 400 bp of sequence homologous to the genomic locus immediately adjacent to the ZFN cut sites, were synthesized *de novo*, subcloned into the EcoRV site of pUC57 and sequence-verified (GenScript, Piscataway, NJ, USA).

Genome targeting. One microgram each of the ZFN plasmids (for SHANK3 targeting) or one vial of ZFN mRNA (for AAVS1 targeting) and 1 μg of targeting vector were introduced into 2×10^6 SA001 human ES cells by electroporation (4D Nucleofector with X Unit, P3 Solution, program DN-100; all from Lonza, Basel, Switzerland), and cells plated in the presence of 10 μM Y-27632. Selection with G418 (Life Technologies) was started 2 days later. After 10 days of selection, resistant colonies were manually isolated, transferred to multiwell plates and separately cultured without selection. Clones with site-specific cassette insertions were

identified by PCRs from genomic DNA with the following oligonucleotide primer pairs: SHANK3 locus, SHANK3_F1+Neo_R and Neo_F+SHANK3_R1; AAVS1 locus, AAVS1_F+Neo_R and Neo_F+AAVS1_R. Correctly targeted clones were further subcloned by limited dilution, expanded and re-analyzed by genomic PCR. Double knockouts were generated by targeting clonal isolates of single knockouts with the same SHANK3-targeting ZFNs and targeting constructs harboring a loxP-flanked PGK-driven puromycin *N*-acetyl-transferase cassette (loxP-PGK-puro-loxP). Selection was with puromycin. All lines were confirmed to be karyotypically normal by G-banding (WiCell, Madison WI, USA). Quantitative PCR analysis was performed to verify SHANK3 expression in the lines generated (Supplementary Figure 9).

Data collection and statistics. All experiments were replicated at least three times, as indicated in the figure legends. We performed quality control on each neuronal culture: if the cells were not at least 80% positive for Tuj1 (neuronal-specific β -iii tubulin marker), the culture was discarded. Cultures were randomly selected for assay and were processed blind. The statistical analysis used is reported in the figure legends. The normal distribution was checked using Kolmogorov–Smirnov test. The statistical analysis was carried out using Prism6 (La Jolla, CA, USA) and SPSS (Coppell, TX, USA).

RESULTS

SHANK3 is expressed during early neuronal development

Human iPSC lines from hair keratinocytes, from two donors diagnosed with ASD and carrying microdeletions of the SHANK3 locus, have been previously described.³² Controls came from neurotypical donors. We used a modified version of 'dual SMAD inhibition' to direct iPSCs along a neuronal pathway. The modification involved the inclusion of XAV (2 μM) and dorsomorphin (1 μM), which we have shown independently to drive differentiation toward an olfactory placodal fate (Figure 1a). By day 26, neuronal-specific β -iii-tubulin positive (Tuj1) neurons could be identified, and by day 70, neurons were positive for synaptic markers. Immunocytochemical analysis of the cells at day 30 of neuralization revealed markers positive for placodal neurons (Lhx6, Gnrh1 and Map2: Figures 1b–e). The cells did not express CTIP2, a marker absent from placodal cells but expressed in dorsal telencephalon. We also performed gene expression analysis for both cortical and olfactory placodal control neurons (Figures 1f and g). Placodal neurons expressed *Gnrh1*, *Nkx2.1* and *TRH* but showed marginal expression of *TBR1* expression, a gene involved in cortical development. The converse expression pattern was seen in cortical neurons: high expression of *TBR1*, and minimal expression of *Gnrh1*, *Nkx2.1* and *TRH*.

A previous study¹⁹ reported a decrease in the number of synaptic puncta in cortical neurons derived from individuals with PMDS. We asked, therefore, whether our cells, with a smaller microdeletion, showed a similar phenotype. We compared the expression of synaptic markers in 70-day-old placodal neurons derived from both control and SHANK3 iPSCs. There were fewer puncta labeled with both presynaptic and postsynaptic markers (Synaptophysin and Homer1) in the SHANK3 patient neurons compared with control (Synaptophysin/50 μm : 94.7 ± 6.7 per 50 μm of SHANK3 neurite vs 208.4 ± 14.0 control and Homer/50 μm : 70.6 ± 6.0 SHANK3 vs 180.3 ± 10.9 control) consistent with published data (Figures 4f–h).

Having confirmed the synaptic deficit, we asked how early during differentiation a phenotype could be observed. First, we asked when during development SHANK3 was expressed. Quantitative PCR of control cells indicated that SHANK3 is expressed at days 15 and 25 in neural progenitors and early postmitotic neurons, respectively. In the SHANK3 cells, expression was lower and delayed. Expression is essentially zero at both day 15 and 25 time points and is still approximately 30-fold lower than control at day 40 (Figure 1h). The western blotting analysis of day 30 neurons confirmed the expression of SHANK3 in both control

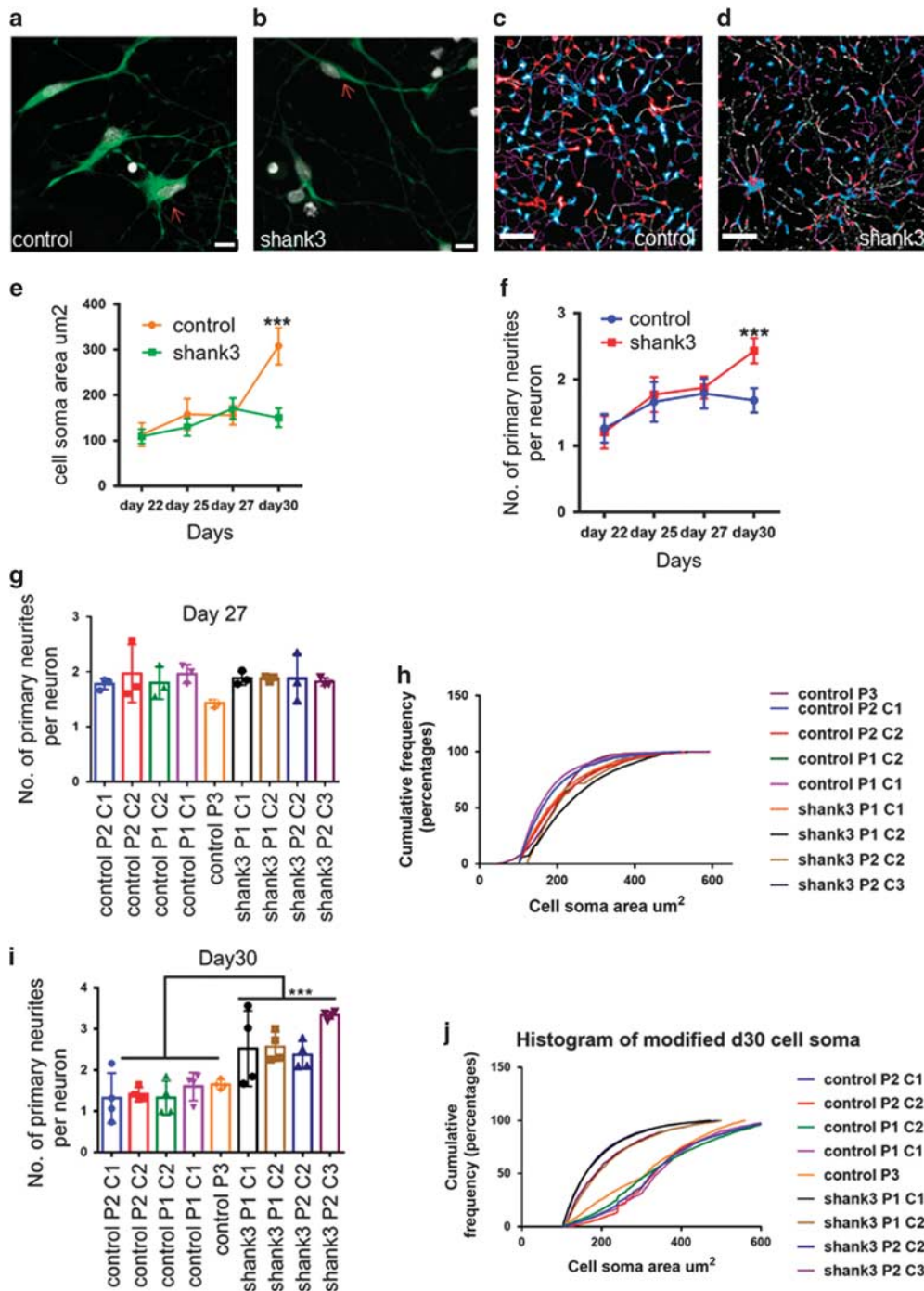


Figure 2. Morphological deficits found in immature SHANK3 patient neurons. **(a)** Control neurons cell soma. **(b)** SHANK3 neurons cell soma (scale = 10 μm , day 30 neurons stained with DCX (doublecortin; green) and DAPI (4,6-diamidino-2-phenylindole; gray)). **(c)** and **(d)** Bare images of Control and SHANK3 DCX⁺ neurons at day 30 taken during high-content screening, scale = 200 μm . **(e)** High-content screening performed to find changes in cell soma area μm^2 from day 22 (late neural progenitors) to day 30 (immature neurons). Data are represented as mean \pm s.e.m., Mann-Whitney *U*-test was performed for each time point; the only difference was seen at day 30. ****P* < 0.001. **(f)** High-content screening performed to find out the number of primary neurites per neuron from day 22 (late neural progenitors) to day 30 (immature neurons). Data are represented as mean \pm s.e.m. Unpaired Student's *t*-test with Welch's correction was performed for each time point; the only difference was seen at day 30. ****P* < 0.001. **(g)** and **(i)** The number of primary neurites per neuron at days 27 and 30. Data are represented as mean \pm s.d., ****P* < 0.001, Student's *t*-test was performed, Control neurons $n = 26.0 \times 10^3$; shank3 neurons $n = 30.0 \times 10^3$. **(h)** and **(j)** Cumulative frequency distribution of cell soma area at days 27 and 30. (****P* < 0.001, Kolmogorov-Smirnov test was performed, Control neurons $n = 26.0 \times 10^3$; shank3 neurons $n = 30.0 \times 10^3$). We performed three biological replicates. We compared five control lines with four SHANK3 lines, three control lines with two clonal replicates and two SHANK3 lines with one clonal replicate of each.

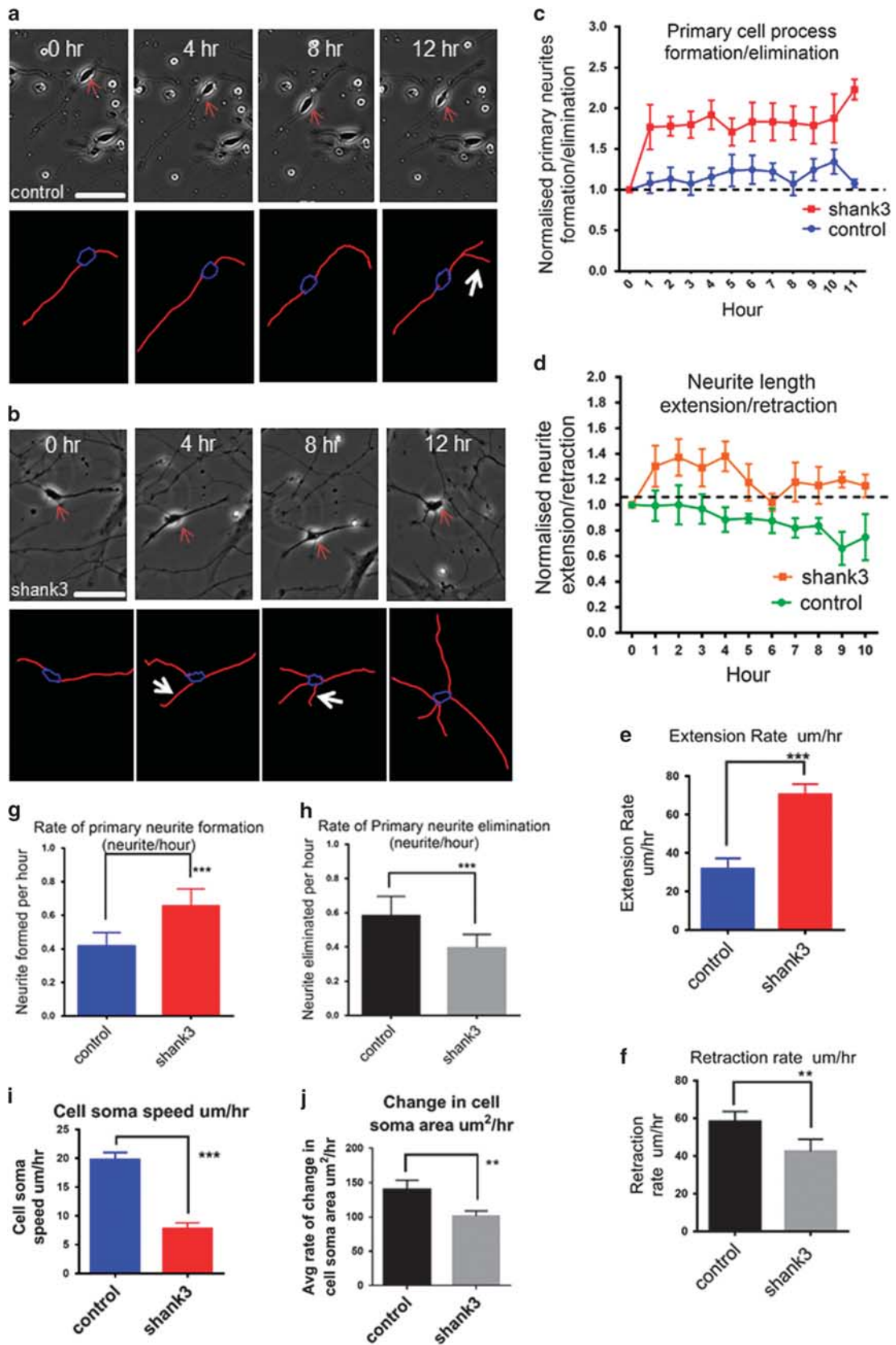


Figure 3. SHANK3 patient neurons exhibit abnormal neurite outgrowth. (a) Phase-contrast image of control neuron and tracing (red: neurite, blue: cell body outline, yellow: secondary branches) neuron at zero hour, fourth hour, eighth hour and twelfth hour. (b) Phase-contrast image of SHANK3 neuron and tracing given below at zero hour, fourth hour, eighth hour and twelfth hour (scale = 50 μm), the arrows represent the neurites formed every hour. (c) Primary neurite of formation/elimination rate were normalized to zero hour; > 1 represents the formation, < 1 represents elimination. Data are presented as mean \pm s.e.m. (Two-way analysis of variance (ANOVA) performed, $***P < 0.001$ b/w genotypes, $***P < 0.001$ b/w genotypes and days). (d) Neurite extension/retraction rate of primary neurite were normalized to zero hour; > 1 represents the extension, < 1 represents retraction. Data are presented as mean \pm s.e.m. ($***P < 0.001$, two-way ANOVA performed). (e) Extension rate ($\mu\text{m h}^{-1}$). (f) Retraction rate ($\mu\text{m h}^{-1}$). (g) Formation rate (neurite h^{-1}). (h) Elimination rate (neurite h^{-1}). Data are represented as mean \pm s.d., $***P < 0.001$, $**P < 0.001$, $***P < 0.001$, $***P < 0.001$ for panels (e–h), respectively. Unpaired Student's *t*-test with Welch's correction was performed. (i) Cell soma speed ($\mu\text{m h}^{-1}$). (j) Change in cell soma area $\mu\text{m}^2 \text{h}^{-1}$. Data are represented as mean \pm s.d. $***P < 0.001$ and $**P = 0.005$ for panels (i) and (j), respectively, unpaired Student's *t*-test with Welch's correction was performed. Control neurons $n = 51$; SHANK3 neurons $n = 59$, from all three biological replicates. We compared four control lines with four SHANK3 lines, two control lines with one clonal replicate of each and two SHANK3 lines with one clonal replicate of each.

and patient lines (Figure 1i). Notably, at day 30 postmitotic neurons appear, and the control neurons showed an increased expression of SHANK3 when compared with SHANK3 patient lines (Supplementary Figure 3A). These results demonstrate that SHANK3 is expressed considerably before the onset of synaptogenesis in these cells and that the shortfall in the expression in the patient lines at these early stages is considerably greater than the twofold difference reported at synaptic stages in the PMDS lines.

Morphogenetic deficits during early development of SHANK3 patient

To observe the neuronal development of placodal cultures, we assessed various morphological aspects of the control and SHANK3 patient neurons. At days 30 and 45 of neuralization, cells were transfected with green fluorescent protein and visualized with fluorescence microscopy. The transfection efficiency was the same for both control and SHANK3 at approximately 2%. We counted: the number of primary neurites per neuron, average neurite length (μm), and average cell soma diameter (μm). At both stages, the cell diameter (μm) was smaller in the SHANK3 neurons while the neurite length (μm) and the mean number of neurites was higher (Supplementary Figure 2E and F (i–iii)).

In order to automate this assay and to assess the entire neuronal population rather than the 2% transfected cells, we configured a high-content cytometry assay to assess these same morphogenetic parameters at four stages of neuralization: days 22 (late neural progenitors), 25, 27, and 30 (immature neurons, Figures 2a–d). No differences were apparent between SHANK3 and control cells at days 22, 25 or 27 (Figures 2e and f). At day 30, however, we observed a significantly smaller cell soma area (Figure 2j) and higher number of primary neurites per neuron (Figure 2i) in the SHANK3 lines compared with control. This confirmed our previous observation on day 30 cells and confirmed this time point as the earliest at which the phenotype could be observed.

Next, we wanted to know whether the morphogenetic deficits we observed were specific to the placodal cells. For this, we generated cortical neurons and compared the structural development in control vs the SHANK3 patient lines. The cortical neurons were CTIP2 positive (Supplementary Figure 4C). The cell soma area and number of primary neurites per neuron were analyzed using high-content imaging at day 30 of neuralization as the placodal cultures. There were no significant differences between the control and SHANK3 patient cortical neurons (Supplementary Figures 4D and E). Analysis of neurite length, however, revealed that the SHANK3 patient cortical neurons had significantly shorter neurites than the controls (Supplementary Figure 4F). These findings in cortical cells concur with the recent study of Yi et al.²⁰

Neurite outgrowth is altered in immature SHANK3 patient placodal neurons

The increased neurite number in SHANK3 patient cells could result from increased neurite formation, decreased elimination or both. We compared the rate of neurite formation and elimination (neurite h^{-1}) and extension and retraction ($\mu\text{m h}^{-1}$) in control and SHANK3 patient neurons at day 30 of neuralization over a 12-h period using time-lapse imaging (Figures 3a and b). The rate of formation of the primary neurite was significantly higher in SHANK3 patient neurons than in controls, whereas the rate of primary neurite elimination was significantly lower (Figures 3c, g and h). There was, however, no difference between the patient and control lines in the rate of secondary branch formation and elimination (Supplementary Figures 4A and B). Similarly, the rate of extension of primary neurite length was significantly higher in SHANK3 patient neurons, whereas the rate of primary neurite length retraction was significantly lower (Figures 3d–f). Thus SHANK3 patient neurons show an increased rate of primary neurite formation and an increase in neurite length extension. This corroborates our finding of increased number and length of primary neurites.

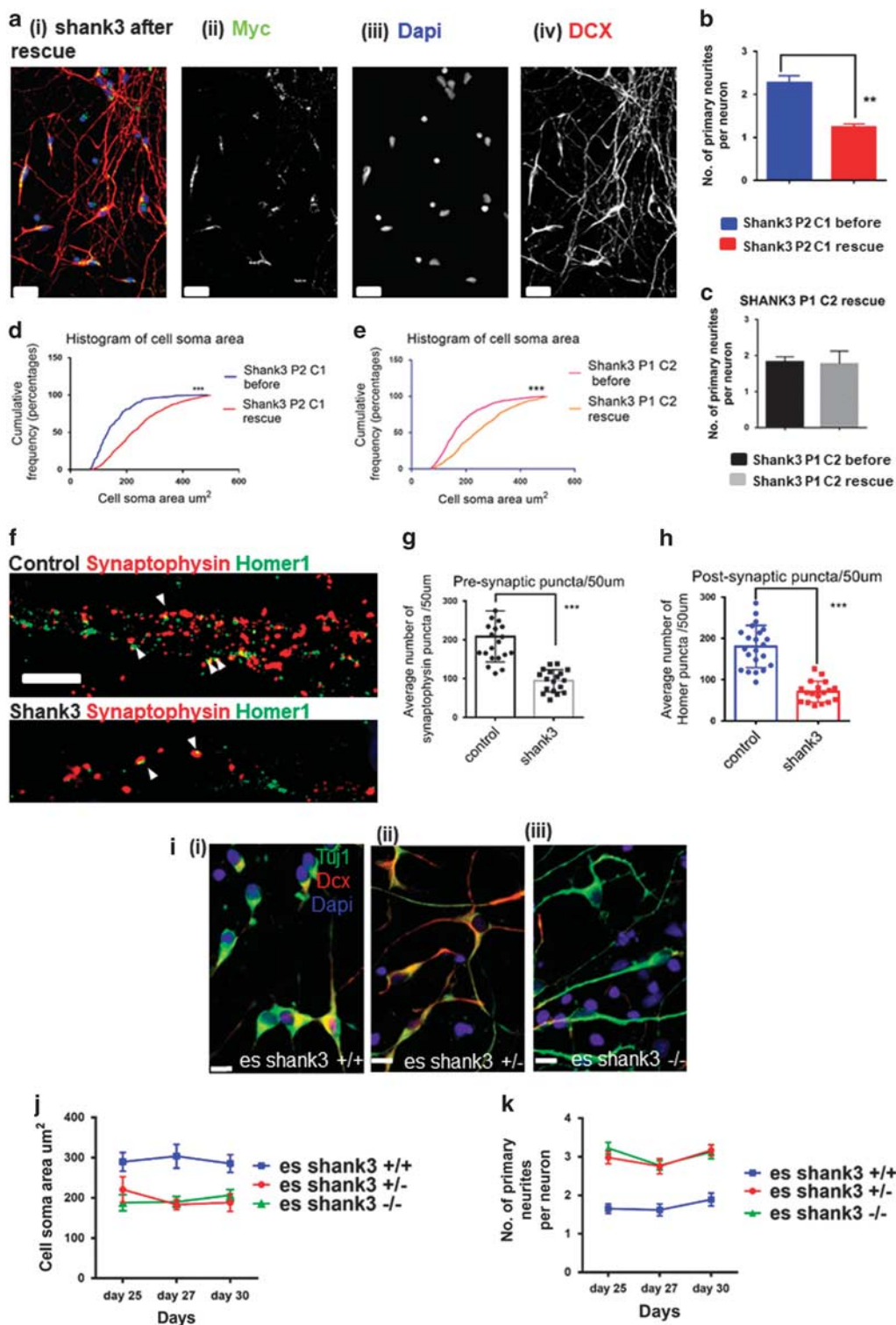
During early development, GnRH neurons pass through the nasal placode to the hypothalamus,³⁴ and this migratory mechanism has been shown to involve the movement of the cell soma along the neurite.^{35,36} Using time lapse, we observed a similar movement of cell somata along neurites. We calculated the speed of the cell soma movement in control and SHANK3 neurons and discovered that the SHANK3 neurons showed a significant reduced soma speed compared with control (Figure 3i).

The time-lapse study also allowed us to analyze in real time the emergence of the difference in cell soma area in neurons from SHANK3 patients. We calculated the average rate of change in cell soma area over the period of 12 h ($\mu\text{m}^2 \text{h}^{-1}$) in control and SHANK3 patient-derived cells and found the rate to be significantly lower in the SHANK3 patient neurons (Figure 3j). Thus the SHANK3 cells grew more slowly than controls.

SHANK3 rescue of the morphogenetic phenotype.

To confirm that the morphogenetic phenotype we have observed was indeed a consequence of SHANK3 haploinsufficiency, we attempted to rescue the phenotype by SHANK3 overexpression. We infected the SHANK3 patient placodal neurons with a lentivirus encoding the full-length SHANK3 (ORF) where the N terminal had been fused to Myc (Supplementary Figure 6). Non-infected SHANK3 neuronal cultures were included as controls. The neurons were infected at day 20/21 of neuralization and the virus was removed after 24 h.

On day 30, neurons were fixed and stained for Myc to identify transduced cells and with anti-DCX to identify immature neurons (Figure 4a). Roughly 80% of neurons were Myc⁺. We programmed the high-content imaging platform to count cells that were positive for Myc and DCX⁺. We measured the cell soma area (μm^2)



and number of primary neurites per neuron using high-content imaging.

In the *SHANK3* patient female line, (*SHANK3* P2 C1) cell soma area increased significantly from 153.2 ± 6.5 to $238.6 \pm 3.7 \mu\text{m}^2$ with *SHANK3* overexpression (Figure 4d). Similarly, the *SHANK3* male patient line (*SHANK3* P1 C2) increased from 180.4 ± 3.2 to $250.4 \pm 4.1 \mu\text{m}^2$ (Figure 4e). Hence, *SHANK3* overexpression rescued the cell soma phenotype. Cells infected with

control Myc-only virus showed no change (Supplementary Figure 3C).

SHANK3 overexpression in *SHANK3* P2 C1 also produced a significant decrease in the primary number of neurites (from 2.27 ± 0.09 to 1.24 ± 0.04 neurites: Figure 5b). However, overexpression in *SHANK3* P1 C2 did not bring about significant change in neurite number (Figure 5c). As both findings were robust, we are currently unable to draw a firm con-

Figure 4. Overexpression of SHANK3 rescues morphogenetic deficits in immature SHANK3 patient neurons: (a) Day 30 SHANK3 neuron after rescue (i), DCX (doublecortin; red) (iv), MYC (green) stained (ii), DAPI (4,6-diamidino-2-phenylindole; blue) (iii), (scale = 25 μm). (b) Number of primary neurites per neuron SHANK3 Patient 2 clone 1 with and without rescue. (c) Number of primary neurites per neuron SHANK3 Patient 1 clone 2 with and without rescue. Data are represented as mean \pm s.e.m. Data compared via unpaired Student's *t*-test with Welch's correction. (***P* = 0.0026 SHANK3 P2 C1 before vs SHANK3 P2 C1 rescue, ***P* = 0.0066 SHANK3 P2 C1 before vs SHANK3 P2 C1 rescue-18). (d) Cumulative frequency distribution of cell soma area (μm^2) of SHANK3 Patient 2 clone 1 with and without rescue. Data compared via Kolmogorov–Smirnov test. (****P* < 0.001 SHANK3 P2 C1 before vs SHANK3 P2 C1 rescue, ****P* < 0.001 SHANK3 P2 C1 before vs SHANK3 P2 C1 rescue-18, ****P* < 0.001 SHANK3 P1 C2 before vs SHANK3 P1 C2 rescue and ****P* < 0.001 SHANK3 P1 C2 before vs SHANK3 P1 C2 rescue-18). SHANK3 P2 C1 before *n* = 331, SHANK3 P2 C1 with rescue *n* = 749, SHANK3 P2 C1 with rescue -18 *n* = 557, SHANK3 P1 C2 before *n* = 689, SHANK3 P1 C2 with rescue *n* = 662, SHANK3 P1 C2 with rescue-18 *n* = 839 from all three biological replicates. (f) Day 70 control neurons stained with Homer1 (postsynaptic marker) and Synaptophysin (presynaptic marker). Day 70 SHANK3 neuron stained with Homer1 (postsynaptic marker) and Synaptophysin (presynaptic marker) (scale = 10 μm), arrows represent the co-localization of pre and post synaptic markers. (g) The average number of Synaptophysin puncta per 50 μm . (h) The average number of Homer1 puncta per 50 μm . Significant differences in expression of both Synaptophysin and Homer1 were found. ****P* < 0.001 (unpaired Student's *t*-test with Welch's correction). Data are expressed as mean \pm s.e.m. We compared two control lines with two SHANK3 lines (control neurons *n* = 46; SHANK3 neurons *n* = 41, from three biological replicates). (i) (i–iii) day 30 es shank3 +/+, es shank3 +/- and es shank3 -/- derived neurons stained with DAPI, DCX and Tuj1 (scale bar = 10 μm). (j) Cell soma area changes through various neuralization stages (days 25–30). Data are represented as mean \pm s.e.m. Friedman's two-way analysis of variance (ANOVA) by ranks pairwise comparison ****P* < 0.001 on all three stages of neuralization. (k) The change in the number of primary neurites (days 25–30). Data are presented as mean \pm s.e.m., (es shank3 shank3+/+ *n* = 5.1×10^3 , es shank3 +/- *n* = 5.0×10^3 , es shank3 -/- *n* = 5.11×10^3 from all three biological replicates). Two-way ANOVA with repeated measure performed at each time point, ****P* < 0.001: significant difference was found between genotypes and ***P* < 0.005: there is an interaction between days and genotypes. Bonferroni's multiple comparisons test revealed ****P* < 0.001 es shank3 +/+ vs es shank3 +/-, ****P* < 0.001 es shank3 +/+ vs es shank3 -/- and *P* = 1.0 es shank3 +/- and es shank3 -/-.

clusion regarding the role of SHANK3 in this aspect of the phenotype.

Morphogenetic deficits reported in SHANK3 homozygous knockout human ES cells

The SHANK3 rescue indicates that the morphogenetic phenotype is a consequence of the reduced SHANK3 expression in the patient cells. To confirm this observation, we compared a human ES line engineered to carry either one or two copies of a SHANK3 mutation discovered in ASD patients (es SHANK3 +/- or es SHANK3 -/-). These lines were compared with the parent ES line (es SHANK3 +/+). Cells were differentiated into placodal neurons and then analyzed using high-content imaging at three stages of neuralization; day 25, 27 and 30 (Figure 4i(i–iii)). At all the three time points, both es shank3 +/- and es shank3 -/- derived neurons had significantly smaller cell soma than the es shank3 +/+ (Figure 4j, Supplementary Figure 5B(i–iii)). Similarly, both the es shank3 +/- and es shank3 -/- neurons had more neurites than the es shank3 +/+ at all three stages (days 25, 27 and 30; Figure 4k, Supplementary Figure 5a(i–iii)). Thus the es cells phenocopied the deficit observed in the SHANK3 patient lines, albeit at an earlier stage, day 25 rather than day 30. This corresponds to our empirical observation that these cells neuralize somewhat faster than the iPSCs.

SHANK3 patient neurons show reduced actin

There are several molecular mechanisms that could be responsible for the observed morphogenetic deficits in SHANK3 patient lines. We know from previous studies that SHANK3 has various actin-binding partners, which regulate the neuronal cytoskeleton. Therefore, we tested whether there were any changes in actin. In Figures 5a–c, we see a reduction in both G and F actin intensity in SHANK3 patient neurons at day 30 neuralization.

Several plausible mechanisms could link this actin phenotype to the morphogenetic findings described above. Densin-180 is known to bind to the N terminal ANK domain of SHANK3 protein and thereby antagonize dendritic branching. SHANK3 binds to the C terminus of densin-180, making the PDZ domain of densin-180 inaccessible to δ catenin. δ catenin binds with densin-180 and is required for the formation of new branches.³⁷ One hypothesis, therefore, is that SHANK3 deficiency leads to more densin-180 being accessible to bind to δ catenin, which leads to an increase in

neurite formation. However, western blotting analysis of at day 30 of neuralization showed no changes in densin-180. Similarly, another actin regulator cortactin, which also binds to SHANK3, showed no changes in protein levels (Supplementary Figures 11C and D). Altered expression of these proteins seems, therefore, not to be part of the mechanism.

Another possibility emerges from a recent study, which showed that SHANK3-deficient mice exhibit a decrease in the levels of β PPIX and this, in turn, leads to a decrease in Rac1/PAK/LIMK activity. A key downstream target of LIMK is cofilin, an actin-depolymerizing factor that is inactivated when phosphorylated by LIMK.^{38–40} So, when levels of LIMK decrease, more cofilin remains in the active state resulting in increased depolymerization of actin. Cofilin severs the actin filaments, which generates more actin filaments or primers. These uncapped filaments are elongated by the Arp2/3 complex. This process helps form neurites.^{41,42}

To test the hypothesis that cofilin is involved in the increased neurite outgrowth observed in the SHANK3 cells, we examined the ratio of phospho-cofilin to cofilin in day 30 neurons in both patient and control lines. The patient cells showed a reduced phospho-cofilin to total cofilin ratio (Figures 5d and e). To impute function, we used a cofilin-blocking peptide (15 pmol g^{-1} —see Duffney *et al.*⁴⁰) at day 30 of neuralization to attempt to rescue the neurite phenotype in the patient cells. Twenty-four hours of treatment with the blocking peptide produces a decrease in the number of neurite as shown in Figures 5f–h. This suggests therefore that the reduced SHANK3 results in a decrease in Rac1/PAK/LIMK activity leading to reduced phospho-cofilin and ultimately increased neurite outgrowth.

DISCUSSION

In this study, we used neural cells from iPSCs derived from ASD patients carrying SHANK3 microdeletions, plus human ES lines engineered to carry SHANK3 mutations, to show both synaptic and morphogenetic anomalies in comparison with control cells. We used a SHANK3 rescue to confirm that both phenotypes are indeed the consequence of the SHANK3 haploinsufficiency.

Previously, studies in both rodents and human iPSC indicate that deletion of SHANK3 disrupts synaptic signaling.^{19,21–25,43,44} The reductions we see in synaptic puncta associated with SHANK3 are consistent with those findings. Phenotypes in earlier neurogenesis have not been observed, however, even though SHANK3 expression

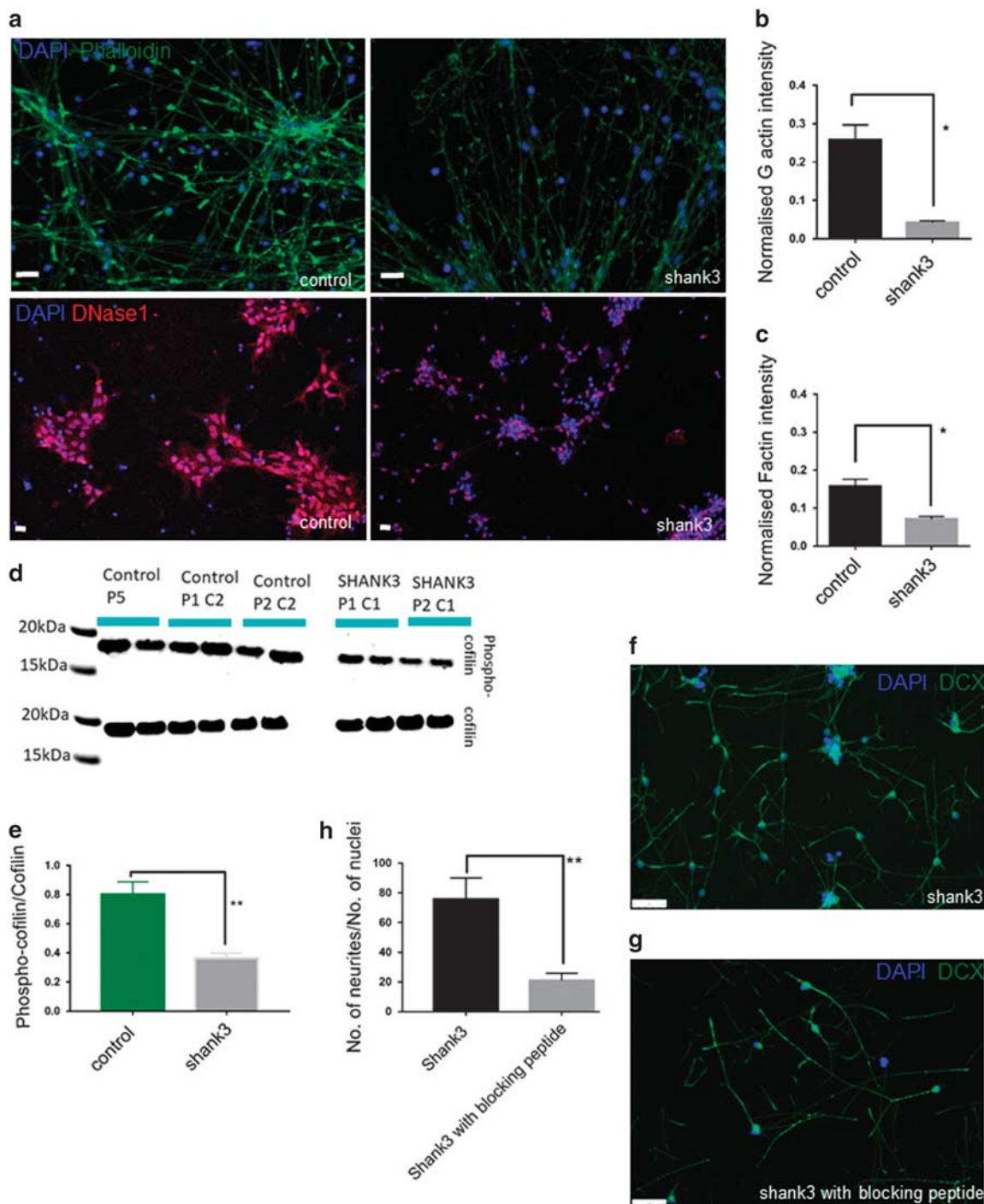


Figure 5. SHANK3 patient neurons show reduced F and G actin. (a) Phalloidin (green, F actin) and Dnase1 (red, G actin) staining of control and SHANK3 patient neurons (Scale = 20 μ m). (b and c) Normalized (G and F) actin intensity. Data are presented as mean \pm s.e.m., * P = 0.029 and * P = 0.0275 for panels (b) and (c), respectively, unpaired Student's t -test with Welch's correction was performed. (d and e) Western blotting of Phospho-Cofilin/total Cofilin. Data are presented as mean \pm s.e.m., ** P = 0.0025, unpaired Student's t -test with Welch's correction was performed. (f and g). SHANK3 neurons at day 30/31 before and after addition of cofilin blocking peptide (scale = 50 μ m). Data are presented as mean \pm s.e.m., ** P = 0.0032, unpaired Student's t -test with Welch's correction was performed.

is known to commence at neural tube stages, at least in *Xenopus*.²⁶ Our study reveals that as SHANK3 patient olfactory placodal neurons first emerge, they develop smaller cell bodies and more and longer primary neurites than the control neurons. Moreover, the SHANK3 neurons have deficits in neurite extension and retraction and reduced motility. Nonetheless, this phenotype is not found in the cortical cells, a result consistent with the recent observations of Yi

et al.²⁰ These results not only suggest that SHANK3 has a role in the regulation of neuronal structure during early morphogenesis but also suggests that this is an area-specific phenomenon as different outcomes are observed in cortical and placodal neurons. We believe our study provides the first evidence for a SHANK3 phenotype, associated with ASD, emerging soon after neurons become postmitotic and considerably before the onset of synaptogenesis.

Smaller cell soma size has been consistently reported in both postmortem and rodent models of ASD.⁴⁵ Both Rett's and Fragile X syndrome show a reduction in cell soma size,^{46–53} and the phenotype is also observed iPSC models of these diseases.^{54–56} The neurite phenotype is also likely to be of importance in ASD. Peça et al.,²⁴ studying the *Shank3* knockout mice, traced Golgi-stained striatal medium spiny neurons and found an increase in total dendritic length. Similarly, Sholl analysis revealed neuronal hypertrophy as measured by increased dendritic arborization. These authors linked this to significant enlargement of caudate in *Shank3* knockout mice. An enlarged caudate in autistic patients is associated with repetitive behavior.^{57,58} Thus it is possible that increased brain volume seen in autistic patients could reflect the morphological changes we report here. Nonetheless, the area specificity of these phenotypes clearly needs further elucidation in cellular and animal models as well as in postmortem material.

A limitation of this study is that we have analyzed only two iPSC lines from each of the two *SHANK3* patients. To consolidate these findings, therefore, we employed genome-edited es lines to show a similar phenotype to that seen in the *SHANK3* iPSC patient lines. Furthermore, we rescued the morphogenetic deficits in the patient cells by *SHANK3* overexpression, confirming the role of *SHANK3* in the genesis of the phenotype. We also confirmed that overexpression of *SHANK3* subsequently increased both presynaptic synaptic and postsynaptic puncta significantly in older *SHANK3* patient neurons (Supplementary Figure 10).

In conclusion, this study presents the novel idea that *SHANK3* haploinsufficiency causes early structural deficits in neurons, which impact synaptic development. Moreover, we show a phenotype arising in olfactory placodal neurons, destined for the hypothalamus, consistent with suggestions of a functional association between ASD and this brain structure. This study has not only defined a critical period during development when cellular deficits occur in ASD but has also determined a period for successful rescue of these deficits.

CONFLICT OF INTEREST

The authors declare no conflict of interest.

ACKNOWLEDGMENTS

We thank the National Institute for Health Research (NIHR) Biomedical Research Centre for Mental Health at South London and Maudsley NHS Foundation Trust and Institute of Psychiatry, King's College London for financial support. This article presents independent research funded by the NIHR. The views expressed are those of the author(s) and not necessarily those of the NHS, the NIHR or the Department of Health. The research leading to these results has received support from the Innovative Medicines Initiative Joint Undertaking under grant agreement nos. 115300 and 115439, resources of which are composed of financial contribution from the European Union's Seventh Framework Programme (FP7/2007–2013) and EFPIA companies' in kind contribution. We also thank the Mortimer D Sackler Foundation for funding this work. We thank our colleagues Victoria Woods, Rosy D'Oyly-Watkins and Rupert Faraway for technical support.

AUTHOR CONTRIBUTIONS

Conceptualization: AK and JP; methodology: AK, DPS, and JP; investigation: AK, PN, RDT, LCA, NJFG, and SA; writing—original draft: AK and JP; writing—review and editing: AK, DPS, and JP; funding acquisition: JP; resources: WL, RG, SA, and DPS; supervision, DPS and JP.

REFERENCES

- Hallmayer J, Cleveland S, Torres A, Phillips J, Cohen B, Torigoe T et al. Genetic heritability and shared environmental factors among twin pairs with autism. *Arch Gen Psychiatry* 2011; **68**: 1095–1102.
- Betancur C. Etiological heterogeneity in autism spectrum disorders: more than 100 genetic and genomic disorders and still counting. *Brain Res* 2011; **1380**: 42–77.
- LaFlamme B. Genetic modules for autism. *Nat Genet* 2015; **47**: 105–105.
- Bourgeron T. A synaptic trek to autism. *Curr Opin Neurobiol* 2009; **19**: 231–234.
- Boeckers TM, Bockmann J, Kreutz MR, Gundelfinger ED. ProSAP/Shank proteins—a family of higher order organizing molecules of the postsynaptic density with an emerging role in human neurological disease. *J Neurochem* 2002; **81**: 903–910.
- Naisbitt S, Kim E, Tu JC, Xiao B, Sala C, Valtschanoff J et al. Shank, a novel family of postsynaptic density proteins that binds to the NMDA receptor/PSD-95/GKAP complex and cortactin. *Neuron* 1999; **23**: 569–582.
- Lim S, Naisbitt S, Yoon J, Hwang J-I, Suh P-G, Sheng M et al. Characterization of the shank family of synaptic proteins: multiple genes, alternative splicing, and differential expression IN brain and development. *J Biol Chem* 1999; **274**: 29510–29518.
- Sheng M, Kim E. The Shank family of scaffold proteins. *J Cell Sci* 2000; **113**(Pt 1): 1851–1856.
- Uchino S, Waga C. SHANK3 as an autism spectrum disorder-associated gene. *Brain Dev* 2013; **35**: 106–110.
- Jiang Y-H, Ehlers MD. Modeling autism by SHANK gene mutations in mice. *Neuron* 2013; **78**: 8–27.
- Bonaglia MC, Giorda R, Mani E, Aceti G, Anderlid B-M, Baroncini A et al. Identification of a recurrent breakpoint within the SHANK3 gene in the 22q13.3 deletion syndrome. *J Med Genet* 2006; **43**: 822–828.
- Durand CM, Betancur C, Boeckers TM, Bockmann J, Chaste P, Fauchereau F et al. Mutations in the gene encoding the synaptic scaffolding protein SHANK3 are associated with autism spectrum disorders. *Nat Genet* 2007; **39**: 25–27.
- Leblond CS, Nava C, Polge A, Gauthier J, Huguet G, Lumbroso S et al. Meta-analysis of SHANK mutations in autism spectrum disorders: a gradient of severity in cognitive impairments. *PLoS Genet* 2014; **10**: e1004580.
- Boccutto L, Lauri M, Sarasua SM, Skinner CD, Buccella D, Dwivedi A et al. Prevalence of SHANK3 variants in patients with different subtypes of autism spectrum disorders. *Eur J Hum Genet* 2013; **21**: 310–316.
- Nemirovsky SI, Córdoba M, Zaiat JJ, Completa SP, Vega PA, González-Morón D et al. Whole genome sequencing reveals a de novo SHANK3 mutation in familial autism spectrum disorder. *PLoS ONE* 2015; **10**: e0116358.
- Betancur C, Buxbaum JD. SHANK3 haploinsufficiency: a 'common' but under-diagnosed highly penetrant monogenic cause of autism spectrum disorders. *Mol Autism* 2013; **4**: 17.
- Costales JL, Kolevzon A. Phelan-McDermid syndrome and SHANK3: implications for treatment. *Neurotherapeutics* 2015; **12**: 620–630.
- Brennan KJ, Simone A, Tran N, Gage FH. Modeling psychiatric disorders at the cellular and network levels. *Mol Psychiatry* 2012; **17**: 1239–1253.
- Shcheglovitov A, Shcheglovitova O, Yazawa M, Portmann T, Shu R, Sebastiano V et al. SHANK3 and IGF1 restore synaptic deficits in neurons from 22q13 deletion syndrome patients. *Nature* 2013; **503**: 267–271.
- Yi F, Danko T, Botelho SC, Patzke C, Pak C, Wernig M et al. Autism-associated SHANK3 haploinsufficiency causes Ih channelopathy in human neurons. *Science* 2016; **352**: aaf2669.
- Wang X, McCoy PA, Rodriguiz RM, Pan Y, Je HS, Roberts AC et al. Synaptic dysfunction and abnormal behaviors in mice lacking major isoforms of Shank3. *Hum Mol Genet* 2011; **20**: 3093–3108.
- Yang M, Bozdagi O, Scattoni ML, Wöhr M, Roulet FI, Katz AM et al. Reduced excitatory neurotransmission and mild autism-relevant phenotypes in adolescent Shank3 null mutant mice. *J Neurosci* 2012; **32**: 6525–6541.
- Bozdagi O, Sakurai T, Papapetrou D, Wang X, Dickstein DL, Takahashi N et al. Haploinsufficiency of the autism-associated Shank3 gene leads to deficits in synaptic function, social interaction, and social communication. *Mol Autism* 2010; **1**: 15.
- Peça J, Feliciano C, Ting JT, Wang W, Wells MF, Venkatraman TN et al. Shank3 mutant mice display autistic-like behaviours and striatal dysfunction. *Nature* 2011; **472**: 437–442.
- Schmeisser MJ, Ey E, Wegener S, Bockmann J, Stempel AV, Kuebler A et al. Autistic-like behaviours and hyperactivity in mice lacking ProSAP1/Shank2. *Nature* 2012; **486**: 256–260.
- Gessert S, Schmeisser MJ, Tao S, Boeckers TM, Kühl M. The spatio-temporal expression of ProSAP/shank family members and their interaction partner LAP-SER1 during *Xenopus laevis* development. *Dev Dyn* 2011; **240**: 1528–1536.
- Kurth F, Narr KL, Woods RP, O'Neill J, Alger JR, Caplan R et al. Diminished gray matter within the hypothalamus in autism disorder: a potential link to hormonal effects? *Biol Psychiatry* 2011; **70**: 278–282.
- Belmonte MK, Allen G, Beckel-Mitchener A, Boulanger LM, Carper RA, Webb SJ. Autism and abnormal development of brain connectivity. *J Neurosci* 2004; **24**: 9228–9231.

- 29 Román GC, Ghassabian A, Bongers-Schokking JJ, Jaddoe VWV, Hofman A, de Rijke YB et al. Association of gestational maternal hypothyroxinemia and increased autism risk. *Ann Neurol* 2013; **74**: 733–742.
- 30 Yau VM, Lutsky M, Yoshida CK, Lasley B, Kharrazi M, Windham G et al. Prenatal and neonatal thyroid stimulating hormone levels and autism spectrum disorders. *J Autism Dev Disord* 2015; **45**: 719–730.
- 31 Baron-Cohen S, Auyeung B, Nørgaard-Pedersen B, Hougaard DM, Abdallah MW, Melgaard L et al. Elevated fetal steroidogenic activity in autism. *Mol Psychiatry* 2015; **20**: 369–376.
- 32 Cocks G, Curran S, Gami P, Uwanogho D, Jeffries AR, Kathuria A et al. The utility of patient specific induced pluripotent stem cells for the modelling of Autistic Spectrum Disorders. *Psychopharmacology (Berl)* 2014; **231**: 1079–1088.
- 33 Shi Y, Kirwan P, Livesey FJ. Directed differentiation of human pluripotent stem cells to cerebral cortex neurons and neural networks. *Nat Protoc* 2012; **7**: 1836–1846.
- 34 Wray S. From nose to brain: development of gonadotrophin-releasing hormone-1 neurones. *J Neuroendocrinol* 2010; **22**: 743–753.
- 35 Hutchins BI, Klenke U, Wray S. Calcium release-dependent actin flow in the leading process mediates axophilic migration. *J Neurosci* 2013; **33**: 11361–11371.
- 36 Hutchins BI, Wray S. Capture of microtubule plus-ends at the actin cortex promotes axophilic neuronal migration by enhancing microtubule tension in the leading process. *Front Cell Neurosci* 2014; **8**: 400.
- 37 Quitsch A, Berhörster K, Liew CW, Richter D, Kreienkamp H-J. Postsynaptic shank antagonizes dendrite branching induced by the leucine-rich repeat protein Densin-180. *J Neurosci* 2005; **25**: 479–487.
- 38 Bamberg JR. Proteins of the ADF/cofilin family: essential regulators of actin dynamics. *Annu Rev Cell Dev Biol* 1999; **15**: 185–230.
- 39 Duffney LJ, Wei J, Cheng J, Liu W, Smith KR, Kittler JT et al. Shank3 deficiency induces NMDA receptor hypofunction via an actin-dependent mechanism. *J Neurosci* 2013; **33**: 15767–15778.
- 40 Duffney LJ, Zhong P, Wei J, Matas E, Cheng J, Qin L et al. Autism-like deficits in Shank3-deficient mice are rescued by targeting actin regulators. *Cell Rep* 2015; **11**: 1400–1413.
- 41 Krause M, Gautreau A. Steering cell migration: lamellipodium dynamics and the regulation of directional persistence. *Nat Rev Mol Cell Biol* 2014; **15**: 577–590.
- 42 Chen Q, Pollard TD. Actin filament severing by cofilin dismantles actin patches and produces mother filaments for new patches. *Curr Biol* 2013; **23**: 1154–1162.
- 43 Vicidomini C, Ponzoni L, Lim D, Schmeisser MJ, Reim D, Morello N et al. Pharmacological enhancement of mGlu5 receptors rescues behavioral deficits in SHANK3 knock-out mice. *Mol Psychiatry* 2017; **22**: 689–702.
- 44 Bidinosti M, Botta P, Krüttner S, Proenca CC, Stoehr N, Bernhard M et al. CLK2 inhibition ameliorates autistic features associated with SHANK3 deficiency. *Science* 2016; **351**: 1199–1203.
- 45 Wegiel J, Flory M, Kuchna I, Nowicki K, Ma SY, Imaki H et al. Neuronal nucleus and cytoplasm volume deficit in children with autism and volume increase in adolescents and adults. *Acta Neuropathol Commun* 2015; **3**: 2.
- 46 Irwin SA, Patel B, Idupulapati M, Harris JB, Crisostomo RA, Larsen BP et al. Abnormal dendritic spine characteristics in the temporal and visual cortices of patients with fragile-X syndrome: a quantitative examination. *Am J Med Genet* 2001; **98**: 161–167.
- 47 Bauman ML, Kemper TL, Arin DM. Pervasive neuroanatomic abnormalities of the brain in three cases of Rett's syndrome. *Neurology* 1995; **45**: 1581–1586.
- 48 Kishi N, Macklis JD. MECP2 is progressively expressed in post-migratory neurons and is involved in neuronal maturation rather than cell fate decisions. *Mol Cell Neurosci* 2004; **27**: 306–321.
- 49 Smrt RD, Eaves-Egenes J, Barkho BZ, Santistevan NJ, Zhao C, Aimone JB et al. Mecp2 deficiency leads to delayed maturation and altered gene expression in hippocampal neurons. *Neurobiol Dis* 2007; **27**: 77–89.
- 50 Asaka Y, Jugloff DGM, Zhang L, Eubanks JH, Fitzsimonds RM. Hippocampal synaptic plasticity is impaired in the Mecp2-null mouse model of Rett syndrome. *Neurobiol Dis* 2006; **21**: 217–227.
- 51 Moretti P, Levenson JM, Battaglia F, Atkinson R, Teague R, Antalffy B et al. Learning and memory and synaptic plasticity are impaired in a mouse model of Rett syndrome. *J Neurosci* 2006; **26**: 319–327.
- 52 Nelson ED, Kavalali ET, Monteggia LM. MeCP2-dependent transcriptional repression regulates excitatory neurotransmission. *Curr Biol* 2006; **16**: 710–716.
- 53 Noutel J, Hong YK, Leu B, Kang E, Chen C. Experience-dependent retinogeniculate synapse remodeling is abnormal in MeCP2-deficient mice. *Neuron* 2011; **70**: 35–42.
- 54 Cheung AYL, Horvath LM, Grafodatskaya D, Pasceri P, Weksberg R, Hotta A et al. Isolation of MECP2-null Rett Syndrome patient hiPS cells and isogenic controls through X-chromosome inactivation. *Hum Mol Genet* 2011; **20**: 2103–2115.
- 55 Marchetto MCN, Carromeu C, Acab A, Yu D, Yeo GW, Mu Y et al. A model for neural development and treatment of Rett syndrome using human induced pluripotent stem cells. *Cell* 2010; **143**: 527–539.
- 56 Ananiev G, Williams EC, Li H, Chang Q. Isogenic pairs of wild type and mutant induced pluripotent stem cell (iPSC) lines from Rett syndrome patients as in vitro disease model. *PLoS ONE* 2011; **6**: e25255.
- 57 Hollander E, Anagnostou E, Chaplin W, Esposito K, Haznedar MM, Licalzi E et al. Striatal volume on magnetic resonance imaging and repetitive behaviors in autism. *Biol Psychiatry* 2005; **58**: 226–232.
- 58 Langen M, Schnack HG, Nederveen H, Bos D, Lahuis BE, de Jonge MV et al. Changes in the developmental trajectories of striatum in autism. *Biol Psychiatry* 2009; **66**: 327–333.



This work is licensed under a Creative Commons Attribution-NonCommercial-NoDerivs 4.0 International License. The images or other third party material in this article are included in the article's Creative Commons license, unless indicated otherwise in the credit line; if the material is not included under the Creative Commons license, users will need to obtain permission from the license holder to reproduce the material. To view a copy of this license, visit <http://creativecommons.org/licenses/by-nc-nd/4.0/>

© The Author(s) 2018

Supplementary Information accompanies the paper on the Molecular Psychiatry website (<http://www.nature.com/mp>)